

ChemComm

Chemical Communications

Accepted Manuscript

This article can be cited before page numbers have been issued, to do this please use: S. R. Mangu and V. Chakrapani, *Chem. Commun.*, 2026, DOI: 10.1039/D6CC01794K.



This is an Accepted Manuscript, which has been through the Royal Society of Chemistry peer review process and has been accepted for publication.

Accepted Manuscripts are published online shortly after acceptance, before technical editing, formatting and proof reading. Using this free service, authors can make their results available to the community, in citable form, before we publish the edited article. We will replace this Accepted Manuscript with the edited and formatted Advance Article as soon as it is available.

You can find more information about Accepted Manuscripts in the [Information for Authors](#).

Please note that technical editing may introduce minor changes to the text and/or graphics, which may alter content. The journal's standard [Terms & Conditions](#) and the [Ethical guidelines](#) still apply. In no event shall the Royal Society of Chemistry be held responsible for any errors or omissions in this Accepted Manuscript or any consequences arising from the use of any information it contains.

COMMUNICATION

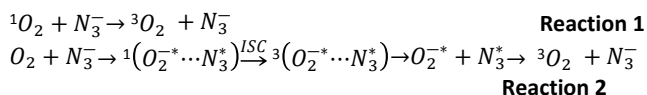
Dual Role of Azide as a Quencher and Stimulator of Singlet Oxygen Generation on Some Manganese Oxides

Shashank Mangu,^a and Vidhya Chakrapani^{a,#}Received 00th January 20xx,
Accepted 00th January 20xx

DOI: 10.1039/x0xx00000x

Sodium azide is a known singlet oxygen (1O_2) quencher in both homogenous and heterogeneous catalytic transformations. We report a paradoxical trend of a strong enhancement in the 1O_2 production during H_2O_2 disproportionation seen on some MnO_x catalyst, specifically layered δ - MnO_2 . Studies with 1O_2 -specific probes show that this activation is due to N_3^- complexation with lattice Mn^{II} of δ - MnO_2 that upon rapid air oxidation produces a metastable surface Mn^{III} -azide complex that strongly catalyzes H_2O_2 disproportionation. In contrast, a bulk Mn^{III} -azide complex does not produce 1O_2 . Due to this dual role, the use of NaN_3 as diagnostic tool for 1O_2 intermediacy should be carefully reconsidered.

Singlet oxygen (1O_2) is a nonradical reactive oxygen species (ROS) known for its high specificity for electrophilic compounds, including biomolecules such as nucleic acids, lipids and proteins, and is exploited in several industrial transformations. A major diagnostic tool for detecting the presence of 1O_2 in aqueous media is using chemicals traps and quenchers. For example, reactive dienes, such as 9,10-disubstituted anthracene, are commonly used traps that selectively react with 1O_2 to form stable endoperoxide adducts that can be detected by mass spectroscopy.¹ In this process, the traps are consumed depending on the rate of 1O_2 formation. On the other hand, physical quenchers that deactivates 1O_2 to triplet oxygen (3O_2) through a radiationless process are the most preferred probes for 1O_2 since the quencher is not consumed and no new products are formed that can contaminate the product stream. Sodium azide (NaN_3) is the most used physical quencher, often used to monitor the presence of 1O_2 . The deactivation process is given:^{2,3}



The rate constant for **Reaction 1** is high with a measured value of $5.0 \times 10^8 \text{ M}^{-1} \text{ s}^{-1}$ in water.⁴ The accepted quenching mechanism obtained from electron spin resonance (ESR) studies is that it proceeds through the formation of a singlet charge transfer complex (**Reaction 2**) in which the electronic charge of N_3^- is partially transferred to

oxygen leading to the formation of radical intermediates of superoxide ($O_2^{\cdot-}$) and azidyl (N_3^*).² This complex undergoes intersystem crossing (ISC) to the triplet ground state with the release of energy (heat) and then dissociates to triplet oxygen (3O_2) with the regeneration of azide anion. Several factors are known to affect this interactive bimolecular quenching rate for the process in homogeneous and heterogeneous systems, such as viscosity⁵, dielectric constant (polarity)⁵, temperature,⁶ ionic strength of the protic solvents,⁷ and the degree of protonation of azide.⁴ Other electron-rich quenching agents, such as amines, also follow this mechanism for 1O_2 . Herein we show that NaN_3 is not a quencher for 1O_2 produced by some MnO_x , specifically δ - MnO_2 containing a high concentration of lattice Mn^{II} . Rather, the presence of N_3^- ions enhance 1O_2 production through the formation of Mn^{III} -azide complex that is highly catalytic towards H_2O_2 disproportionation.

We performed tests with several Mn and non-Mn based oxide catalysts that were otherwise efficient 1O_2 generators in the absence of azide. These include stoichiometric V_2O_5 , δ - MnO_2 , acid treated hexagonal δ - MnO_2 (H- δ - MnO_2), $(La_{0.8}Sr_{0.2})_{0.95}MnO_{3-\delta}$ (henceforth LaSrMnO₃), $LiMn_2O_4$, and La_2NiO_4 .⁸ Two 1O_2 -sensitive fluorogenic probes were used: 1,3 diphenylbenzofuran (DPBF) and singlet oxygen sensor green (SOSG). DPBF is the most used and well-characterized 1O_2 probe due to its high fidelity against 1O_2 photosensitization. It strongly absorbs light at $\sim 410 \text{ nm}$ and emits bright blue fluorescence ($\sim 480 \text{ nm}$) that is proportionally quenched when it reacts with 1O_2 to form an endoperoxide or 1,2-dibenzoylbenzene that is not fluorescent. The rate constant for this reaction is high, with a value of $2.3 \times 10^9 \text{ M}^{-1} \text{ s}^{-1}$ in an ethanol / water (50/50 v/v) mixture.⁹ In a typical run, 1 mg of catalyst was first incubated with $30 \mu\text{M}$ of probe along with NaN_3 (if present) to achieve stable coverage and then reacted with 10-40 μM of H_2O_2 . The emission intensity of the supernatant only after centrifugation was measured. While a decrease in the DPBF intensity is indicative of extent of 1O_2 generation, a decrease can also be caused by the removal of DPBF molecules from the solution due to its adsorption

^a Howard P. Isermann Department of Chemical and Biological Engineering
Rensselaer Polytechnic Institute, Troy, NY-12180

^b # Email: chakrv@rpi.edu.



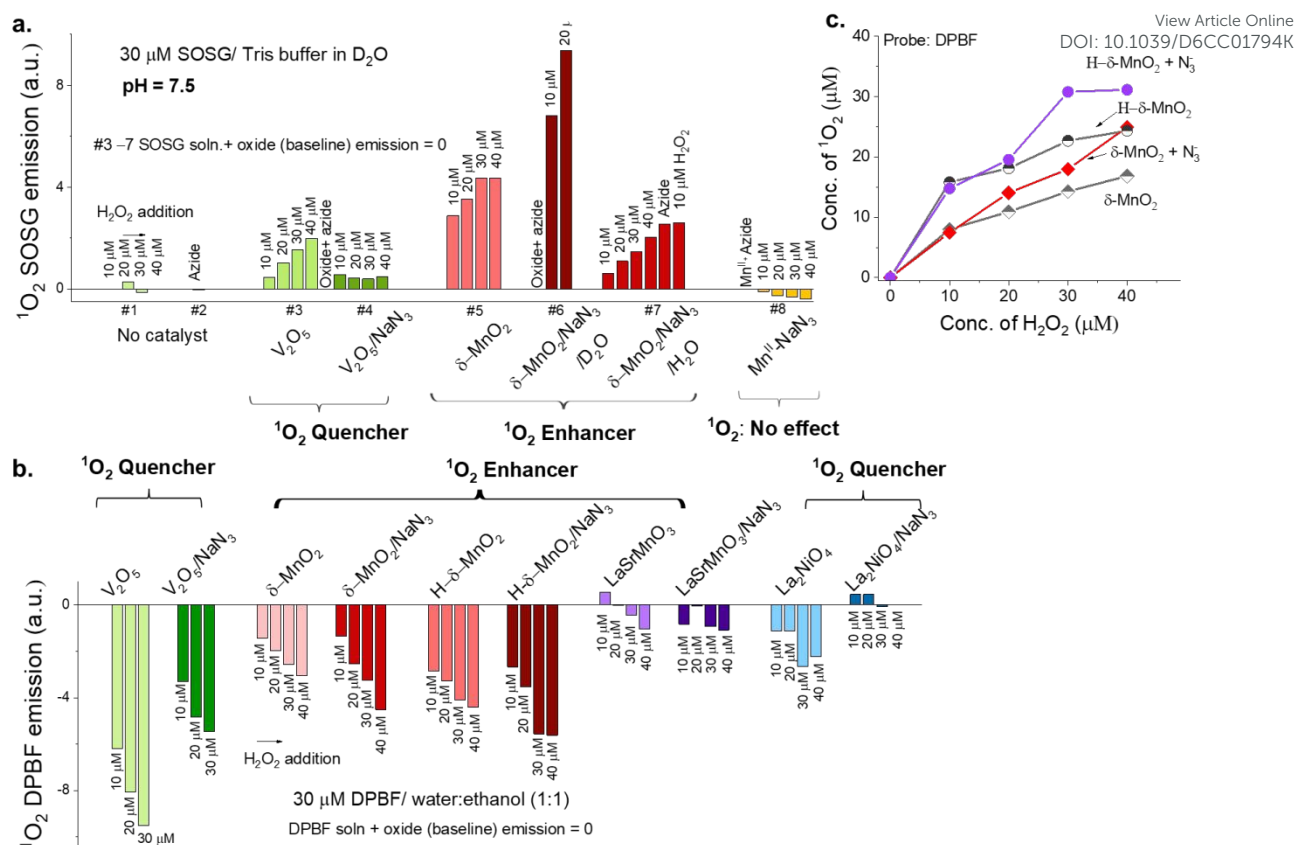


Figure 1. Contrasting trends in $^1\text{O}_2$ -related SOSG (a) and DPBF (b) emissions as well as $^1\text{O}_2$ production (c) caused by the presence of NaN_3 in the electrolyte exposed to V_2O_5 , $\delta\text{-MnO}_2$, and other oxide powders in the presence of 10–40 μM H_2O_2 concentrations. Also shown is the effect of H_2O_2 addition to the bulk Mn^{III} -azide complex. Oxide weight = 1 mg/ml. $[\text{NaN}_3] = 15 \text{ mM}$.

on the catalyst. Therefore, for incontrovertible evidence for $^1\text{O}_2$ production, we used a second probe, SOSG, which shows a positive increase in emission, unlike DPBF that shows an emission decrease, upon reaction with $^1\text{O}_2$. In this case, any SOSG adsorption on the catalyst surface will only lead to a decrease and not an increase in the emission intensity. SOSG is made up of a fluorescein-type fluorophore and an anthracene-derived trapping moiety. In the absence of $^1\text{O}_2$, the fluorophore's emission of the fluorophore is quenched by internal transfer from the anthracene moiety. However, after the reaction of the anthracene moiety with $^1\text{O}_2$, which forms an endoperoxide that is no longer an efficient intramolecular electron donor, the fluorescence of the fluorophore is restored in proportion to the concentration of $^1\text{O}_2$. Furthermore, SOSG is also insensitive to ROS such as OH^* or $\text{O}_2^{\cdot-}$ and has a high fidelity unless when exposed to UV radiation.^{10, 11} All SOSG tests were done with non-UV excitation wavelength of 405 nm in 0.1 M Tris buffer made with D_2O or H_2O . DPBF tests were performed in a 1:1 (v/v) ethanol/water mixture due to its limited solubility in water.

Initial tests of N_3^- effect on the $^1\text{O}_2$ production were performed with V_2O_5 and $\delta\text{-MnO}_2$ as catalysts. V_2O_5 was chosen because it is known to disproportionate H_2O_2 to $^1\text{O}_2$.¹² Single-crystalline V_2O_5 nanostructures were grown using hot filament chemical vapor deposition process.^{13, 14} $\delta\text{-MnO}_2$ was prepared by wet precipitation of KMnO_4 solution using HCl. **Figure 1a** shows the change in the emission intensity of $^1\text{O}_2$ -sensitive SOSG solution. The baseline emission of the supernatant without any H_2O_2 was taken as zero. One observes that for both oxides in the absence of N_3^- , the SOSG emission increases with increasing H_2O_2 concentrations (test #3 and

#5), with $\delta\text{-MnO}_2$ displaying higher activity for $^1\text{O}_2$ generation than V_2O_5 . In the presence of N_3^- , contrasting trends are observed. In V_2O_5 , the presence of N_3^- , which was added prior to the addition of H_2O_2 , caused significant quenching of the $^1\text{O}_2$ signal (test #4), which decreased by 75% with the addition of 15 mM of NaN_3 compared to case without N_3^- . This is as expected and indicates that N_3^- act as a $^1\text{O}_2$ quencher. In contrast, the addition of H_2O_2 to azide-containing buffer with $\delta\text{-MnO}_2$ led to a dramatic increase of $^1\text{O}_2$ signal by 120% (test #6), compared to the same test without azide. This suggests that N_3^- induces $^1\text{O}_2$ production in $\delta\text{-MnO}_2$. Note that neither N_3^- nor H_2O_2 alone in the absence of oxide catalyst cause any change in the emission intensity of the probe (test #1 and #2). This shows the N_3^- -stimulated $^1\text{O}_2$ generation seen with $\delta\text{-MnO}_2$ is not due to reaction with the probe. The $^1\text{O}_2$ generation was confirmed using $\text{D}_2\text{O}/\text{H}_2\text{O}$ isotope effect. The lifetime of $^1\text{O}_2$ in H_2O is only 2.5 μs but increases nearly 10 times ($\sim 20 \mu\text{s}$) in D_2O .^{15, 16} The solvent-induced quenching of $^1\text{O}_2$ is most efficient when the infrared vibrational frequencies of the solvent (e.g. H_2O) coincide with the energy of $^1\Delta \rightarrow ^3\Sigma$ transition of O_2 , thus causing deactivation by transferring the correct quanta of energy.¹⁶ In D_2O , vibrational frequencies shift, and $^1\text{O}_2$ energy transfer becomes less efficient.¹⁶ Consistent with this, the intensity of the $^1\text{O}_2$ signal observed with $\delta\text{-MnO}_2$ and H_2O_2 was almost 3.5–4.5 times higher in D_2O than that observed in H_2O with all other parameters being the same (tests #5 & #7). This confirms that SOSG emissions observed with H_2O_2 decomposition are in fact related to $^1\text{O}_2$. Furthermore, similar measurements probing N_3^- -induced $^1\text{O}_2$ generation resulted in the dramatic decrease in the enhancement of SOSG intensity when H_2O instead of D_2O was used as the solvent (test #7). The SOSG signal increased only 1.5% with



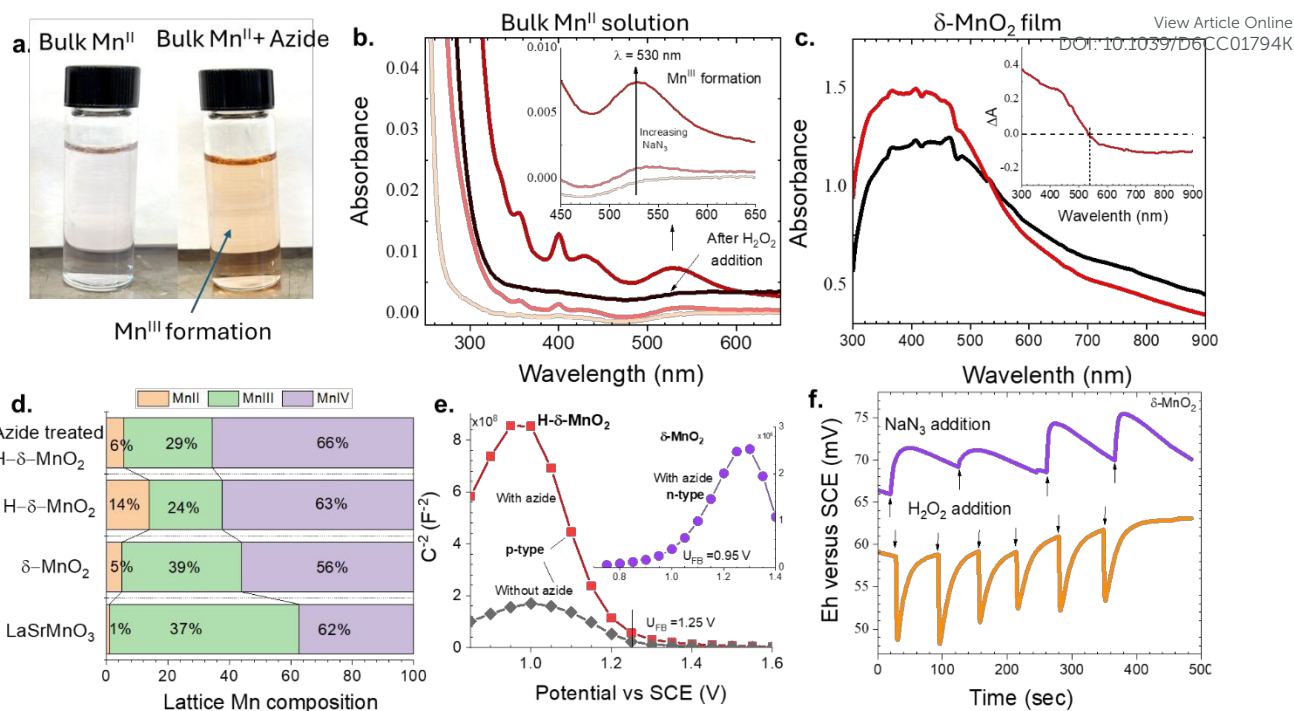


Figure 2. a&b) Photographs and absorption spectrum of bulk Mn^{II} solution with the addition of NaNO₃; c) In-situ changes in the absorption spectrum of δ -MnO₂ due to NaNO₃ addition; d) Comparison of lattice Mn cation composition of pristine and azide-treated Mn oxide powders obtained from PL spectroscopy; e) Mott Schottky plots of H- δ -MnO₂ and δ -MnO₂ (inset) in the presence/absence of azide; and f) Changes in the Eh (OCP) of δ -MnO₂ film upon sequential addition of 15 mM NaNO₃ and then 10 μ M of H₂O₂ pulses.

H₂O₂ addition with H₂O as a solvent compared to 94% observed in D₂O. This is additional evidence for the ¹O₂ formation.

Although SOSG tests confirmed the effect of azide-induced activation, the amount of ¹O₂ produced could not be calculated due to the lack of information on the probe sensitivity factor. Hence, runs were performed using DPBF, a more well-studied probe⁹. The testing was also extended to LiMn₂O₄, La₂NiO₄, and LaSrMnO₃, and H- δ -MnO₂ that also good ¹O₂ generators⁸ to test the quenching/stimulating effects of N₃⁻. **Figures 1b & 1c** compare DPBF emission changes of the supernatant and ¹O₂ produced for various oxides with and without the presence of azide. The results indicate that V₂O₅ followed by H- δ -MnO₂ are the most active catalysts for the disproportionation of H₂O₂ disproportionation to ¹O₂ among the oxides tested in the ethanol/water mixture. The addition of azide again produces contrasting trends. In δ -MnO₂ and LaSrMnO₃ to a smaller extent (**Fig.1b & Fig.S1**), NaNO₃ addition stimulates ¹O₂ generation, as seen from the dramatic decrease in emission intensity with increasing concentrations of H₂O₂ in the presence of azide. However, only a marginal decrease in emission intensity is observed with other oxides, such as La₂NiO₄ (**Fig.1b & Fig.S1**) and LiMn₂O₄ (**Fig.S1**). Thus, NaNO₃ acts as a quencher for ¹O₂ on these catalysts like that seen in V₂O₅. The quenching effects of NaNO₃ in these catalysts compared to the stimulating effect seen in δ -MnO₂ indicates that the mere presence of Mn is not the cause of the contrasting effects. **Fig.1c** plots the ¹O₂ concentration calculated from calibration curve and sensitivity factor⁹ as a function of H₂O₂ concentration. The presence of azide leads to an increase in ¹O₂ production only in δ -MnO₂. We also evaluated the effect of the composition of δ -MnO₂ on the stimulating effects of NaNO₃. The acid treatment of δ -MnO₂ (H- δ -MnO₂) at pH =3 is known to increase the Mn^{II} and Mn vacancy concentrations in the lattice and switch in conductivity from n-type

to p-type.¹⁷ **Figs.1b&1c** show that, even in the absence of N₃⁻, H- δ -MnO₂ has a higher catalytic activity for H₂O₂ to ¹O₂ conversion than δ -MnO₂. In the presence of N₃⁻, the ¹O₂ is further enhanced, much more than that seen with δ -MnO₂. Therefore, the presence of Mn^{II}/vacancy leads to an enhancement of azide stimulation.

It is known that N₃⁻ can act as a bridging ligand by complexing with Mn^{II} ions in bulk to form coordination compounds, such as tri- and tetranuclear clusters.¹⁸ Mn^{II}-azide complexes in bulk undergo a slow oxidation in air-saturated solutions to form the Mn^{III}-azide complex that has a visible absorption peak at 430 nm.^{19,20} We confirmed this by adding a 1-3 mM NaNO₃ solution directly to air-saturated 0.1 M Mn^{II}SO₄ under ambient conditions. As shown in **Fig.2a**, the initially light pink solution of Mn^{II} turned into increasing shades of dark orange upon oxidation, which is characteristic of the Mn^{III}-azide complex. The absorbance spectrum (**Fig.2b**) shows a marked increase in visible light absorbance between 430-530 nm that increases with an increase in NaNO₃ concentration (**Inset of Fig.2b**). This peak is characteristic of Mn^{III} complexes, such as Mn^{III}-pyrophosphate at 480 nm, and Mn^{III}-ethylenediaminetetraacetic acid at 464 nm, respectively.²¹ Therefore, it is possible that the N₃⁻ can bind to the lattice Mn^{II} of δ -MnO₂ catalyst that after rapid oxidation in air forms a metastable Mn^{III}-azide complex that catalyses the disproportionation of H₂O₂ to ¹O₂. To confirm this, we monitored *in-situ* the absorbance change of a δ -MnO₂ film with the addition of 15 mM of NaNO₃ solution (**Fig.2c**). The spectrum taken immediately after NaNO₃ addition shows a marked increase in absorbance at wavelength less than 530 nm, as also evident in $\Delta A = A_{\delta\text{-MnO}_2, \text{NaNO}_3} - A_{\delta\text{-MnO}_2}$ spectrum (**inset**), which provide clear evidence for lattice Mn^{III} formation. To understand why N₃⁻-induced ¹O₂ enhancement is specific to δ -MnO₂, we analysed the lattice Mn cation composition of different MnO_x through X-ray photoelectron spectroscopy and photoluminescence spectroscopy (PL), as detailed elsewhere²², and



is summarized in **Fig.S3** and **Fig.2d**. LaSrMnO₃ has the highest concentration of Mn^{III} (37%) and the lowest concentration of Mn^{II} (1%) in the lattice. Whereas δ-MnO₂ has the highest Mn^{II} content in its lattice (5%), which after acid treatment increases further to 14%. Given that H-δ-MnO₂ shows a higher enhancement in the N₃⁻ induced ¹O₂ production than that seen in δ-MnO₂, the effect of N₃⁻ is likely correlated with the increased presence of Mn^{II} in the lattice. After azide treatment, the lattice Mn^{III} concentration of H-δ-MnO₂ increased from 24% to 29%, while the Mn^{II} concentration decreased from 14% to 6%. This is further confirmation that Mn^{II} after azide treatment is converted to Mn^{III}. The lower azide-induced ¹O₂ production seen other MnO_x may be related to a fewer Mn^{II} lattice sites for azide complexation. The observation that azide-treated H-δ-MnO₂ is much more catalytic towards ¹O₂ production than azide-treated δ-MnO₂ as well as LaSrMnO₃ with its high Mn^{III} content indicates that freshly formed surface Mn^{III} on a δ-MnO₂ structure is more active for H₂O₂ disproportionation. Note that when H₂O₂ was added to the bulk Mn^{III}-azide complex in the presence of SOSG (test #8, **Fig.1**) the intensity of ¹O₂-related SOSG signal decreased rather than increased with H₂O₂ addition. Therefore, the bulk Mn^{III}-azide does not catalyse H₂O₂ disproportionation to ¹O₂.

These different quenching/stimulating effects of azide on ¹O₂ may be related to the differences in thermodynamic redox potential. The redox potential of ¹O₂/H₂O₂ reaction, $U_{1O_2/H_2O_2}^0$, is 0.77 V versus the standard hydrogen electrode (SHE) at pH = 7 for H₂O₂ and ¹O₂ concentrations of 10 μM. The redox potential of Mn^{III} – N₃⁻ / Mn^{II} – N₃⁻ complex in the bulk is only 0.66 V²³ and therefore, cannot induce H₂O₂ disproportionation to ¹O₂, as observed here. On the other hand, V₂O₅, δ-MnO₂ and H-δ-MnO₂ are known to be semiconductors with high work function and electron affinity values (5.6-6 eV),^{17, 24} which is also influenced by different ligands in the electrolyte.^{17, 21} The flat band potential (U_{FB}) determined from the Mott-Schottky (M-S) plots (**Fig.2e**) of δ-MnO₂ and H-δ-MnO₂ are 1.2 V and 1.5 V versus SHE, respectively, with the former and the latter being n-type and p-type semiconductors, respectively. These U_{FB} values are more positive than $U_{1O_2/H_2O_2}^0$, which explains why both materials have a high catalytic activity for ¹O₂ production from H₂O₂. In the presence of azide, the bulk U_{FB} does not shift significantly, indicating that azide does not modulate the bulk electronics properties. However, its addition leads to a positive shift in the oxidation-reduction potential (E_h, **Fig.2f**) or open circuit potential (OCP), which is more reflective of the surface Fermi level (E_F) changes.²⁵ This E_h value corresponds to the relative difference between the surface potential of δ-MnO₂, equivalent to E_F under band bending conditions, and the reference electrode.²⁵ The concomitant increase in the lattice Mn^{III} content suggests that the Mn^{III} formation causes a decrease in the surface E_F position, thus producing an even greater driving force for e⁻ injection from ¹O₂/H₂O₂ reaction. Mn^{III} is also the active site for H₂O oxidation.²⁶ Consistent with this, the addition of H₂O₂ to the aqueous azide solution in contact with δ-MnO₂ results in a negative shift in E_h, implying an increase in the surface E_F position. This is as expected since e⁻ injection would lead to an increase in E_F energy and a conversion of Mn^{III} to back to Mn^{II} (**Fig.2b**).

In summary, this study reports an unusual improvement in the efficiency of H₂O₂ disproportionation on δ-MnO₂ to ¹O₂ in the presence of NaN₃, which paradoxically is a known ¹O₂ quencher in bulk solution for most other catalysts. This activation is shown to be due to N₃⁻ complexation with lattice Mn^{II} of δ-MnO₂ that upon rapid air oxidation, produces a metastable surface Mn^{III}-azide complex that strongly catalyses H₂O₂ disproportionation under neutral conditions.

ACKNOWLEDGEMENTS

The authors are grateful for financial support provided by the Howard P. Isermann fellowship and the Rensselaer Polytechnic Institute.

Conflict of Interest

All authors declare that they have no conflicts of interest.

DATA AVAILABILITY

The data supporting this article have been included as part of the Supplementary Information. Supplementary information: Emission spectrum, calibration curves, and experimental details.

REFERENCES

- J. Tang, J. Chen, Z. Zhang, Q. Ma, X. Hu, P. Li, Z. Liu, P. Cui, C. Wan, Q. Ke, L. Fu, J. Kim, T. Hamada, Y. Kang and Y. Yamauchi, *Chem. Sci.*, 2023, **14**, 13402-13409.
- J. R. Harbour and S. L. Issler, *J. Am. Chem. Soc.*, 1982, **104**, 903-905.
- C. Schweitzer and R. Schmidt, *Chem. Rev.*, 2003, **103**, 1685-1758.
- W. R. Haag and T. Mill, *Photochem. Photobiol.*, 1987, **45**, 317-321.
- N. Miyoshi, M. Ueda, K. Fuke, Y. Tanimoto, M. Itoh and G. Tomita, *Zeitschrift für Naturforschung B*, 1982, **37**, 649-652.
- M. Li, C. S. Cline, E. B. Koker, H. H. Carmichael, C. F. Chignell and P. Bilski, *Photochem. Photobiol.*, 2001, **74**, 760-764.
- M. A. Rubio, D. O. Mártire, S. E. Braslavsky and E. A. Lissi, *J. Photochem. Photobiol. A: Chem.*, 1992, **66**, 153-157.
- S. Mangu and V. Chakrapani, *J. Phys. Chem. C*, 2026, **130**, 6180-6191.
- T. Entradas, S. Waldron and M. Volk, *J. Photochem. Photobiol. B, Biol.*, 2020, **204**, 111787.
- X. Ragàs, A. Jiménez-Banzo, D. Sánchez-García, X. Batllori and S. Nonell, *Chem. Commun.*, 2009, DOI: 10.1039/b822776d, 2920-2922.
- H. Liu, P. J. Carter, A. C. Laan, R. Eelkema and A. G. Denkova, *Sci. Rep.*, 2019, **9**, 8393.
- F. Natalio, R. André, A. F. Hartog, B. Stoll, K. P. Jochum, R. Wever and W. Tremel, *Nat. Nanotechnol.*, 2012, **7**, 530-535.
- S. Lee, Q. Wang and V. Chakrapani, *Phys. Rev. Mater.*, 2024, **8**, 125801.
- V. Chakrapani, M. Brier, A. Puntambekar and T. DiGiovanni, *J. Mater. Res. Focus Issue Early Career Scholar in Material Science*, 2016, **31**, 17.
- N. Miyoshi, M. Ueda, K. Fuke, Y. Tanimoto, M. Itoh and G. Tomita, *Z. Naturforsch. B*, 1982, **37**, 649-652.
- P. B. Merkel and D. R. Kearns, *J. Am. Chem. Soc.*, 1972, **94**, 7244-7253.
- C. Wang, N. Smieszek and V. Chakrapani, *Chem. Mater.*, 2021, **33**, 7805-7817.
- M. Shee and N. P. Singh, *Chem. Soc. Rev.*, 2022, **51**, 2255-2312.
- H. D. Moya, E. A. Neves, M. E. Vázquez and N. Coichev, *Talanta*, 1996, **43**, 67-72.
- H. D. Moya, E. A. Neves and N. Coichev, *Spectroscopy Letters*, 2001, **34**, 537-547.
- C. Wang and V. Chakrapani, *ACS Earth Space Chem.*, 2023, **7**, 774-787.
- V. Chakrapani, C. Wang, Q. Wang and N. Smieszek, *Surf. Interface Anal.*, 2022, **54**, 1192-1202.
- H. D. Moya, E. A. Neves and N. Coichev, *Talanta*, 1997, **44**, 797-803.



Journal Name

COMMUNICATION

24. S. Lee, Q. Wang and V. Chakrapani, *J. Appl. Phys.*, 2024, **136**, 205101.
25. V. Chakrapani, in *Metal Ions and the Route to Life*, eds. W. Nitschke and S. Duval, CRC Press, Boca Raton, 1st edn., 2025, DOI: 10.1201/9781003459910-7, p. 24.
26. I. Roy, C. Wang, N. Smieszek, X. Li, L. Tsapatsaris and V. Chakrapani, *ChemSusChem*, 2022, **15**, e202200062.

View Article Online
DOI: 10.1039/D6CC01794K



DATA AVAILABILITY

The data supporting this article have been included as part of the Supplementary Information. Supplementary information: Emission spectrum, Calibration curves and further experimental details.

